Hyperoside prevents osteoporosis by activating the PI3K/AKT signaling pathway to inhibit oxidative stress and promote osteogenesis

LIRONG LI[1,2], HUAIDONG DENG[1], SHABIN ZHUAN[1], BOYU WU[1,2] and DAWEI XIAO[1]

[1]Department of Orthopedics, Dongguan Traditional Chinese Medicine Hospital, Dongguan, Guangdong 523000, P.R. China; [2]Department of Orthopedics, Guangzhou University of Chinese Medicine, Guangzhou, Guangdong 510405, P.R. China

Received May 13, 2025; Accepted October 24, 2025

DOI: 10.3892/mmr.2025.13767

Abstract. Hyperoside (Hyp), a naturally occurring flavonol glycoside derived from *Crataegus*, otherwise known as hawthorn, possesses potent antioxidant properties and has demonstrated therapeutic potential in various oxidative stress-related diseases, including osteoporosis (OP). However, the precise molecular mechanisms underlying the anti-osteoporotic effects of Hyp remain to be fully elucidated. The present study aimed to evaluate the therapeutic efficacy of Hyp against OP and to elucidate its underlying mechanisms. An osteoporotic mouse model was established via bilateral ovariectomy (OVX) to assess the *in vivo* efficacy of Hyp. Network pharmacology was employed to predict the potential therapeutic targets of Hyp in OP. *In vitro* experiments using bone marrow mesenchymal stem cells (BMSCs) were performed to validate the findings. Techniques including alkaline phosphatase staining, Alizarin red S staining, reverse transcription-quantitative PCR and western blotting were used to assess osteogenic differentiation and molecular signaling pathways. Micro-CT analysis revealed that Hyp significantly ameliorated OVX-induced bone loss in mice. Network pharmacology identified the PI3K/AKT signaling pathway as a potential key target. *In vitro*, Hyp significantly reduced H_2O_2-induced oxidative stress in BMSCs and promoted their osteogenic differentiation. Mechanistically, Hyp was found to activate the PI3K/AKT signaling pathway, suggesting its notable role in mediating the antioxidant and osteoinductive effects of Hyp. Summarily, Hyp may effectively alleviate OVX-induced OP in mice, potentially by mitigating oxidative stress and promoting osteogenesis via activation of the PI3K/AKT signaling pathway. These findings provide novel insights into the therapeutic mechanism of Hyp and support its potential as a candidate agent for OP treatment.

Correspondence to: Professor Dawei Xiao, Department of Orthopedics, Dongguan Traditional Chinese Medicine Hospital, 3 Dongcheng Section, Songshan Lake Avenue, Dongguan, Guangdong 523000, P.R. China
E-mail: 17722384380@163.com

Key words: osteoporosis, hyperoside, PI3K/AKT signaling pathway, oxidative stress

Introduction

Osteoporosis (OP) is a systemic skeletal disorder characterized by reduced bone mass and deterioration of bone microarchitecture, resulting in increased bone fragility and a higher risk of fractures. This condition markedly impairs the quality of life of affected patients and may even lead to increased mortality rates (1). As the global population ages at an accelerating rate, the incidence of OP continues to increase. In China alone, the number of individuals aged ≥60 years is >210 million, posing considerable challenges for the prevention and management of OP (2). Therefore, the development of effective therapeutic strategies is of substantial clinical importance.

Currently, clinical treatments for OP primarily include pharmacological therapy, exercise interventions and physical therapies (3,4). However, each of these approaches presents notable limitations. For example, while bisphosphonates effectively inhibit bone resorption, long-term use has been associated with adverse effects such as osteonecrosis of the jaw and gastrointestinal disturbances (5). Similarly, hormone replacement therapy may increase the risk of cardiovascular events and breast cancer in certain patient populations (6,7). Therefore, the development of novel and safer therapeutic strategies remains an important focus in current OP research.

In previous years, oxidative stress has emerged as a notable contributor to the pathogenesis of OP. Factors such as aging, iron overload and estrogen deficiency can disrupt the balance between oxidative and antioxidant systems in the body, leading to excessive accumulation of reactive oxygen species (ROS) (8,9). These elevated ROS levels cause oxidative damage to key macromolecules including DNA, lipids and proteins, thereby accelerating cellular apoptosis (10). In the context of OP, oxidative stress modulates signaling pathways, cytokine expression and protein activity in bone marrow mesenchymal stem cells (BMSCs), osteoblasts and osteoclasts (11). Oxidative stress impairs the osteogenic differentiation potential of BMSCs, inhibits osteoblast mineralization, and promotes the activation, proliferation and maturation of osteoclasts (12,13).

This leads to a disrupted balance between bone formation and resorption, impairs bone remodeling and ultimately accelerates the progression of OP (14).

The research on natural drugs for the treatment of OP has recently attracted widespread attention (15,16). Hyperoside (Hyp), as a natural flavonoid compound existing in various plants, such as *Crataegus*, *Apocynum venetum* and *Hypericum perforatum*, exhibits multiple pharmacological activities. Previous studies have demonstrated that Hyp has a protective effect on the cardiovascular and nervous systems (17,18). However, the therapeutic effect and mechanism of Hyp on OP remain insufficiently characterized. Therefore, the present study aimed to explore the therapeutic effect and molecular mechanism of Hyp on OP, providing new ideas and a theoretical basis for the treatment of OP through a combination of *in vivo* and *in vitro* experiments.

Materials and methods

Reagents. Hyp (cat. no. HY-N0452) and LY294002 (cat. no. HY-10108) were purchased from MedChemExpress with a purity of 99.5%. The RNA extraction kit (cat. no. AG21207) was selected from Hunan Accurate Bio-Medical Technology Co., Ltd. Primer synthesis was completed by Sangon Biotech Co., Ltd. The Cell Counting Kit-8 (CCK-8) (cat. no. C0037), alkaline phosphatase (ALP) staining kit (cat. no. C3206) and Alizarin red S (ARS) staining kit (cat. no. C0148S) were all purchased from Beyotime Biotechnology. The primary antibodies runt-related transcription factor 2 (Runx2) (cat. no. AF5186, rabbit), Osterix (cat. no. DF7731, rabbit), β-actin (cat. no. AF7018, rabbit), phosphorylated (p)-PI3K (cat. no. AF3242, rabbit), PI3K (cat. no. AF6241, rabbit), AKT (cat. no. AF0832, rabbit), p-AKT (cat. no. AF0016, rabbit), as well as the corresponding HRP-conjugated goat anti-rabbit IgG secondary antibody (cat. no. S0001), were all purchased from Affinity Biosciences. Isoflurane (cat. no. R510-22-10) was purchased from Shenzhen Ruiwode Life Science Co., Ltd.

Animal experimentation. A total of 40 female C57BL/6J mice were purchased from the Guangdong Provincial Medical Experimental Center [license no. SCXK(YUE)2022-0002]. Female mice (age, 8 weeks; weight, 20-25 g) were randomly divided into control, model, low-concentration and high-concentration groups (n=10 each) and housed in the specific pathogen-free-grade Experimental Animal Center of The First Affiliated Hospital of Guangzhou University of Chinese Medicine (Guangzhou, China). The housing conditions were as follows: 22-25˚C; 40-60% humidity; 12-h light/dark cycle; *ad libitum* access to food/water. After 1 week of acclimation, except for the control group, bilateral ovariectomy (OVX) was performed under isoflurane inhalation anesthesia (5% for induction and 2% for maintenance via precision vaporizer), with depth confirmed by loss of pedal reflex. At 1-week post-surgery, the low- and high-concentration groups were intragastrically administered 40 and 80 mg/kg Hyp, respectively, and the control and model groups received an equal volume of vehicle (0.9% NaCl containing <0.1% DMSO), once daily for 8 weeks. The selected doses were based on a previous study reporting osteoprotective effects of Hyp in ovariectomized mice (19). Humane endpoints were defined as >20% weight loss, inability to access food or water, severe distress or moribund state; health and behavior were monitored daily. Euthanasia was performed by deep anesthesia with 5% isoflurane followed by cervical dislocation, with death confirmed by absence of heartbeat, respiration and corneal reflex. The total experimental duration was 10 weeks. No unexpected deaths occurred, and all procedures were approved by the Animal Experiment Ethics Committee of The First Affiliated Hospital of Guangzhou University of Chinese Medicine (approval no. GZTCMF1-202403241).

Micro-CT scanning. The lower limbs of mice were positioned on the scanning table of the MicroCT scanner (SkyScan 1276; Bruker-Michrom, Inc.), with scanning parameters set to appropriate values, including a voltage of 50 kV, a current of 200 μA and a scanning resolution of 9 μm. The scan was subsequently performed. After the scan was completed, specific reconstruction algorithms in the scanning software were used to reconstruct the two-dimensional projection images into three-dimensional images. Subsequently, CT-analyser (CTAn) software (version 1.17.7.2; Bruker-Michrom, Inc.) was used for data analysis. Initially, the scan data were imported into the CTAn software, the appropriate region of interest (ROI) was selected, typically starting with the distal femoral growth plate, and 150 slices were analyzed upwards of this ROI (Fig. S1). Using the standard analysis function in CTAn, parameters such as trabecular thickness (Tb.Th), trabecular separation (Tb.Sp), trabecular number (Tb.N) and bone volume fraction (BV/TV) were calculated. Based on set threshold values, the software automatically identified bone and non-bone tissues and generated data for the aforementioned bone structure parameters. Finally, the analysis results were exported and the parameters compared between different groups to further analyze trends and variations.

Hematoxylin and eosin (H&E) and tartrate-resistant acid phosphatase (TRAP) staining. The mouse lower limb bone tissue samples were rinsed with PBS (Gibco; Thermo Fisher Scientific, Inc.) and then fixed in 4% paraformaldehyde at 4˚C for 24 h. Subsequently, they were immersed in the decalcification solution for 2 weeks for decalcification, followed by rinsing with distilled water. After that, the samples were dehydrated with successive concentrations of alcohol and treated with xylene for permeabilization. Subsequently, the bone tissues were embedded in paraffin, trimmed and cut into 5-μm sections. The sections were placed in a 63˚C constant temperature oven for baking for 2 h. During the H&E staining process, the sections were first dewaxed and hydrated, then stained with hematoxylin solution for 5 min at room temperature (22-25˚C). After differentiation with hydrochloric acid alcohol and bluing with tap water, the sections were stained with eosin solution for 2 min at room temperature. Finally, the sections were dehydrated with a gradient alcohol series, permeabilized with xylene and sealed with neutral balsam. Images were then captured using a light microscope (CX43; Olympus Corporation).

For TRAP staining, the sections were similarly dewaxed and rehydrated. TRAP staining was performed using a commercial TRAP staining kit (cat. no. G1492; Beijing Solarbio Science &

Technology Co., Ltd.) according to the manufacturer's instructions. Briefly, the sections were incubated in TRAP working solution containing naphthol AS-BI phosphate and Fast Red Violet LB salt in the presence of sodium tartrate at 37˚C for 1 h in the dark. After washing with distilled water, the sections were counterstained lightly with hematoxylin, then dehydrated, cleared in xylene and sealed with neutral balsam. TRAP-positive osteoclasts appeared as red or purplish-red multinucleated cells located along the trabecular bone surface. Representative images were obtained under a light microscope, and osteoclast number was semi-quantitatively evaluated by counting the number of TRAP-positive cells per field under standardized magnification.

Acquisition of Hyp action targets. The structure of Hyp was obtained from the PubChem database (https://pubchem.ncbi.nlm.nih.gov/) and then imported into the SwissTargetPrediction (http://www.swisstargetprediction.ch/), PharmMapper (http://www.lilab-ecust.cn/pharmmapper/), Super-Pred (https://insilico-cyp.charite.de/SuperCYPsPred/) and TargetNet (http://targetnet.scbdd.com/) databases to predict its potential protein targets. After removing duplicates and unannotated targets, all candidate targets were imported into the UniProt database (https://www.uniprot.org/) using the parameters 'reviewed', '*Homo sapiens*' and 'gene name primary' to standardize the target names into official gene symbols. This approach has been widely applied in previous network pharmacology studies (20,21).

Prediction of OP targets and differential gene analysis. The Gene Expression Omnibus database (https://www.ncbi.nlm.nih.gov/geo/) was searched using 'osteoporosis' as the key word, and the species '*Homo Sapiens*' was selected to obtain the GSE35956 (22) gene chip dataset and the GSE80614 (23). gene chip dataset. In R software (version 4.3.1; The R Foundation for Statistical Computing), the parameters $P<0.05$ and |log (fold change) |>2 were set to screen for differential genes and draw a volcano plot. Subsequently, searches and screenings were conducted in the GeneCards (https://www.genecards.org/) and Online Mendelian Inheritance in Man databases (https://www.omim.org/) using the aforementioned key word. Finally, the datasets were integrated and duplicates were removed to obtain the disease-target dataset.

Acquisition of potential action targets of Hyp for treating OP. To conduct an in-depth study and elucidate the interaction mechanisms of the active ingredients of Hyp in the intervention and treatment of OP, a Venn analysis was performed between the action targets of the active ingredients of Hyp and OP-related targets. The overlapping region represents the potential targets of the Hyp for treating OP. Subsequently, a Venn diagram was generated to visualize these intersecting targets.

Construction of the protein-protein interaction (PPI) network and screening of core targets. The intersecting targets between the OP and the Hyp were imported into the Search Tool for the Retrieval of Interacting Genes/Proteins (STRING) database (https://string-db.org/) for PPI analysis. Briefly, the intersecting target proteins were imported into the STRING database, the organism was set to *Homo sapiens*, and the database query was performed to generate the PPI network. This process was used to construct a PPI network model, thereby facilitating the understanding of cellular functional interactions between protein expression profiles and enabling a deeper comprehension of protein functions at the cellular level. Following retrieval, the PPI network diagram was exported and its corresponding '.tsv' format file was downloaded. The '.tsv' file was then imported into Cytoscape (version 3.9.1; https://cytoscape.org/) and the topological parameters of each node in the network were analyzed using the CytoNCA plugin. Target importance within the network was evaluated from three dimensions: Node connectivity, betweenness centrality and closeness centrality. Finally, a core target screening network was constructed to identify the core targets.

Enrichment analysis of Gene Ontology (GO) biological functions and Kyoto Encyclopedia of Genes and Genomes (KEGG) information transmission pathways of core targets. The Metascape database (https://metascape.org) enables enrichment of target genes into their associated genomes and signaling pathways, annotates gene functions, visualizes enrichment analysis results and standardizes genes with different identification codes. To further elucidate the gene functions of the screened targets and their involvement in signaling pathways, these targets were imported into the Metascape database for GO functional enrichment analysis and KEGG pathway enrichment analysis. The Metascape database was used to visualize the enrichment analysis results. Based on ascending P-values, the top 10 results from each GO category and the top 20 KEGG pathways were selected and visualized using the platform.

Cell culture. Mouse primary BMSCs (cat. no. MIC-BIOSPECIES-s018) were purchased from Guangzhou Xinyuan Biotechnology Co., Ltd. The cells were cultured in α-Minimum Essential Medium (Gibco; Thermo Fisher Scientific, Inc.) supplemented with 10% fetal bovine serum (Gibco; Thermo Fisher Scientific, Inc.) and 1% penicillin-streptomycin. Cultures were maintained in a humidified incubator at 37˚C with 5% CO_2. The medium was refreshed every 2 days. Once the cells reached 80-90% confluence, they were detached using 0.25% trypsin-EDTA and passaged at a ratio of 1:3. Cells at passages 3-6 were used for all subsequent experiments.

CCK-8 assay. The cells were seeded into a 96-well plate at a density of $5x10^3$ cells/well and cultured overnight to allow adherence. For the Hyp cytotoxicity assay, the cells were treated with different concentrations of Hyp (0, 10, 20, 40 and 80 μM) for 24 h at 37˚C. For the oxidative stress model, the cells were exposed to H_2O_2 at concentrations of 50, 100, 200 or 400 μM for 24 h at 37˚C to evaluate the dose-dependent cytotoxicity. To assess the protective effects of Hyp, the cells were pretreated with different concentrations of Hyp (10, 20 and 40 μM) for 24 h, followed by exposure to 200 μM H_2O_2 for 4 h at 37˚C. After each treatment, 10 μl CCK-8 solution (Beyotime Biotechnology) was added to each well and incubated for 1 h at 37˚C. Finally, a microplate reader was used to measure the absorbance at 450 nm.

5-Ethynyl-2'-deoxyuridine (EDU) assay. An EDU incorporation assay (cat. no. C0075S; Beyotime Biotechnology) was performed to evaluate the proliferation of BMSCs. Briefly, BMSCs were pretreated with Hyp (20 or 40 μM) for 24 h at 37˚C, followed by exposure to H_2O_2 (200 μM) for 4 h at 37˚C. After treatment, the cells were washed three times with PBS. Then, BMSCs were incubated with EDU for 2 h at 37˚C. The EDU working solution was prepared by diluting 10 mM EDU stock with culture medium to a final concentration of 10 μM. Following EDU incubation, the cells were fixed with 4% paraformaldehyde for 15 min at room temperature. Cells were then washed three times with PBS for 5 min each. After fixation, the cells were permeabilized with 0.3% Triton X-100 in PBS for 15 min and were subsequently washed again with wash buffer. EDU incorporation was detected using an EDU detection kit, and the proliferating cells were analyzed using a fluorescence microscope.

ALP staining and ARS staining. BMSCs were seeded into 12-well plates. After cell attachment to the surface, they were categorized into groups and subjected to the respective interventions. Osteogenic induction was initiated using an osteogenic induction medium containing 10 nM dexamethasone, 50 μg/ml vitamin C and 10 mM β-sodium glycerophosphate. The cells were divided into: i) A control group; ii) a model group treated with 200 μM H_2O_2; iii) a low-concentration group treated with 20 μM Hyp and 200 μM H_2O_2; and iv) a high-concentration group treated with 40 μM Hyp and 200 μM H_2O_2. The culture medium was refreshed every 3 days. ALP staining was performed on day 7. The cells were rinsed three times with PBS, fixed with 4% paraformaldehyde for 30 min at room temperature, and then stained using an ALP staining kit at 37˚C for 30 min. ARS staining was conducted on day 14. The cells were washed three times with PBS, fixed with 4% paraformaldehyde for 30 min at room temperature, and then stained with ARS at room temperature for 30 min. To quantitatively evaluate the degree of mineralization, the ARS stain was eluted with 10% w/v cetylpyridinium chloride for 1 h, and the OD value at 570 nm was measured using a microplate reader. All images were captured under a light microscope (Olympus Corporation), and quantitative analysis of mineralization intensity was performed using ImageJ software (version 1.8.0; National Institutes of Health).

Measurement of ROS level. The present study employed DCFH-DA to detect intracellular ROS levels. After the aforementioned cell intervention was completed, DCFH-DA (cat. no. S0033S; Beyotime Biotechnology) was diluted to a final concentration of 10 μM in serum-free medium and incubated at 37˚C in the dark for 30 min. The cells were then rinsed three times with PBS, and images were captured under a fluorescence microscope. For flow cytometric detection of ROS, after the incubation, the cells were gently washed once with PBS to remove any excess fluorescent probe that had not entered the cells. The cells were then digested with trypsin and collected into centrifuge tubes. Following centrifugation (300 x g, 5 min, 4˚C), the supernatant was discarded and 500 μl of PBS was added to resuspend the cells. The resulting cell suspension was transferred into flow cytometry tubes and analyzed on a BD FACSCalibur flow cytometer (BD Biosciences). Data were processed using FlowJo software (version 10.8.1; BD Biosciences).

Measurement of superoxide dismutase (SOD) and malondialdehyde (MDA). The BMSCs were seeded into 6-well plates. Once the cells had adhered to the well surface, they were subjected to intervention according to the aforementioned grouping for a duration of 24 h. Upon completion of the intervention, cell samples from each group were harvested. For the determination of intracellular SOD level, the working solution was prepared according to the protocol of the SOD activity detection kit (cat. no. S0101; Beyotime Biotechnology). After incubation at 37˚C for 30 min, the absorbance at 450 nm was measured using a microplate reader. The SOD activity in the cell samples of each group was then calculated based on the standard curve. For the detection of MDA levels, the working solution was prepared according to the instructions of the MDA detection kit (cat. no. S0131; Beyotime Biotechnology). After thorough mixing with the samples, the mixture was heated at 100˚C for 15 min, cooled to room temperature in a water bath and centrifuged at 1,000 x g for 10 min at room temperature. A total of 200 μl supernatant was transferred into a 96-well plate, and the absorbance was measured at 532 nm using a microplate reader. The MDA content in the cell samples of each group was then calculated based on the standard curve.

Reverse transcription-quantitative PCR (RT-qPCR). The cell treatments were performed as aforementioned, and total RNA was extracted from BMSCs using an RNA extraction kit (cat. no. AG21207; Hunan Accurate Bio-Medical Technology Co., Ltd.) according to the manufacturer's protocol. After measuring the concentration, the RNA was reverse transcribed into cDNA using the PrimeScript RT reagent kit (cat. no. RR047A; Takara Bio, Inc.) with the following temperature protocol: 37˚C for 15 min, 85˚C for 5 sec, and hold at 4˚C. qPCR was performed using a SYBR® Green qPCR Mix (cat. no. AG11761; Hunan Accurate Bio-Medical Technology Co., Ltd.). Using the cDNA of each group as the template, and after adding the buffer and primers, PCR amplification was performed according to the following parameters described in the instruction manual: Initial denaturation at 95˚C for 30 sec, followed by 40 cycles of denaturation at 95˚C for 5 sec and annealing/extension at 60˚C for 40 sec, in accordance with the manufacturer's instructions. With *18S rRNA* as the internal control, the relative mRNA expression levels were calculated using the $2^{-\Delta\Delta Cq}$ method (24). The primer pair sequences for *18S rRNA*, *Runx2*, *Alp*, *Osterix* and type I collagen *(Col1)* are listed in Table I.

Western blot analysis. The BMSCs were treated as aforementioned. Total proteins were extracted from BMSCs using RIPA lysis buffer (cat. no. P0013B; Beyotime Biotechnology) supplemented with a protease and phosphatase inhibitor cocktail (cat. no. P1005; Beyotime Biotechnology). Proteins were quantified by BCA assay and 30 μg total protein was loaded per lane. Proteins were separated by SDS-PAGE on 10% gels, then transferred to PVDF membranes (cat. no. IPVH00010; MilliporeSigma). After blocking with 5% skim milk in TBS containing 0.1% Tween-20 (TBST) for 2 h at room temperature, the membranes were incubated overnight at 4˚C with

Table I. Primer sequences.

Gene	Forward (5'-3')	Reverse (5'-3')
18s	TGGTTGCAAAGCTGAAACTTAAAG	AGTCAAATTAAGCCGCAGGC
Runx2	GCCGGGAATGATGAGAACTA	GGACCGTCCACTGTCACTTT
Alp	CCAGAAAGACACCTTGACTGTGG	TCTTGTCCGTGTCGCTCACCAT
Col1	CCTCAGGGTATTGCTGGACAAC	CAGAAGGACCTTGTTTGCCAGG
Osterix	GGCTTTTCTGCGGCAAGAGGTT	CGCTGATGTTTGCTCAAGTGGTC

Alp, alkaline phosphatase; *Runx2*, runt-related transcription factor 2; *Col1*, type I collagen.

primary antibodies: Runx2 (1:1,000), Osterix (1:1,000), PI3K (1:1,000), p-PI3K (1:1,000), AKT (1:1,000), p-AKT (1:1,000) and β-actin (1:5,000). Following three washes with TBST, membranes were incubated with HRP-conjugated secondary antibodies (1:5,000) for 1.5 h at room temperature. After further TBST washes, protein bands were visualized using ECL Chemiluminescence Detection Kit (cat. no. 170-5061; Bio-Rad Laboratories, Inc.). Band densities were semi-quantified using ImageJ software (version 1.8.0; National Institutes of Health).

Immunohistochemistry. Paraffin-embedded mouse femur sections, prepared as aforementioned for H&E and TRAP staining, were used for immunohistochemical analysis. Briefly, the femurs were fixed in 4% paraformaldehyde for 24 h at room temperature, decalcified in 10% EDTA solution (pH 7.4) for 2 weeks, dehydrated, embedded in paraffin and cut into 5-μm sections. After the sections had been dewaxed, antigen retrieval was performed. The sections were then treated with 3% H_2O_2 to block endogenous peroxidase activity, followed by blocking with 5% normal goat serum (cat. no. C0265; Beyotime Biotechnology) for 30 min at room temperature. The sections were incubated overnight at 4˚C with the following primary antibodies: p-PI3K (cat. no. AF3242; 1:200) and p-AKT (cat. no. AF0016; 1:200) (all from Affinity Biosciences). The primary antibody was applied and incubated overnight at 4˚C. On the following day, after thorough washing with PBS, the corresponding secondary antibody (1:200; cat. no. S0001; Affinity Biosciences) was applied and incubated at room temperature for 2 h. The sections were subsequently developed using a DAB chromogenic agent (cat. no. P0203; Beyotime Biotechnology), counterstained with hematoxylin for 3 min at room temperature, dehydrated, cleared and mounted. The staining results were observed and analyzed under a light microscope (Olympus Corporation), and five random non-overlapping fields per section were selected for semi-quantitative analysis using ImageJ software (version 1.8.0; National Institutes of Health).

Inhibitor treatment. To investigate the protective effects of Hyp and the involvement of the PI3K/AKT signaling pathway, BMSCs were divided into four groups: Control, model (H_2O_2), Hyp and Hyp + LY294002. Cells in the control group were cultured under standard conditions without any treatment. Cells in the model group were exposed to 200 μM H_2O_2 for 4 h at 37˚C to induce oxidative stress. In the Hyp group, cells were pretreated with Hyp (40 μM) for 24 h at 37˚C, followed by 200 μM H_2O_2 treatment for 4 h. To verify the role of the PI3K/AKT signaling pathway, cells in the Hyp + LY294002 group were pretreated with the PI3K inhibitor LY294002 (10 μM; MedChemExpress) for 2 h at 37˚C before Hyp intervention. After pretreatment, the cells were exposed to Hyp (40 μM) for 24 h and were subsequently treated with H_2O_2 (200 μM) for 4 h at 37˚C. LY294002 was dissolved in DMSO, and the final DMSO concentration in the culture medium did not exceed 0.1% (v/v).

Statistical analysis. Statistical analyses were performed using SPSS version 25.0 (IBM Corp.). Data are presented as the mean ± standard deviation. Each experiment was independently repeated at least three times. Differences among multiple groups were evaluated by one-way analysis of variance (ANOVA). When significant differences were detected by ANOVA, Tukey's honestly significant difference post hoc test was applied for pairwise comparisons. $P<0.05$ was considered to indicate a statistically significant difference.

Results

Hyp alleviates OP in mice induced by OVX. The present study utilized micro-CT and H&E staining to comprehensively assess structural alterations in the lower limb bones of mice. Compared with in the control group, the model group exhibited significant reductions in Tb.N, Tb.Th and BV/TV, alongside a significant increase in Tb.Sp (Fig. 1A-E). These findings validated the successful establishment of the OP model. Following Hyp administration, these parameters significantly improved in a dose-dependent manner, indicating that Hyp effectively promoted trabecular bone formation, mitigated OVX-induced bone loss and contributed to the restoration of bone microarchitecture.

Histological evaluation by H&E staining further corroborated these observations. In the OVX group, trabeculae were sparse and attenuated, the marrow cavity was markedly expanded, osteocyte density was reduced and cell morphology appeared irregular (Fig. 1F). Additionally, the number of empty lacunae was markedly elevated. By contrast, bone sections from Hyp-treated mice exhibited more intact and compact trabeculae, an increased number of osteocytes with normalized morphology and a reduction in empty lacunae.

To further investigate cellular changes, the present study quantitatively analyzed osteoblast and osteoclast populations.

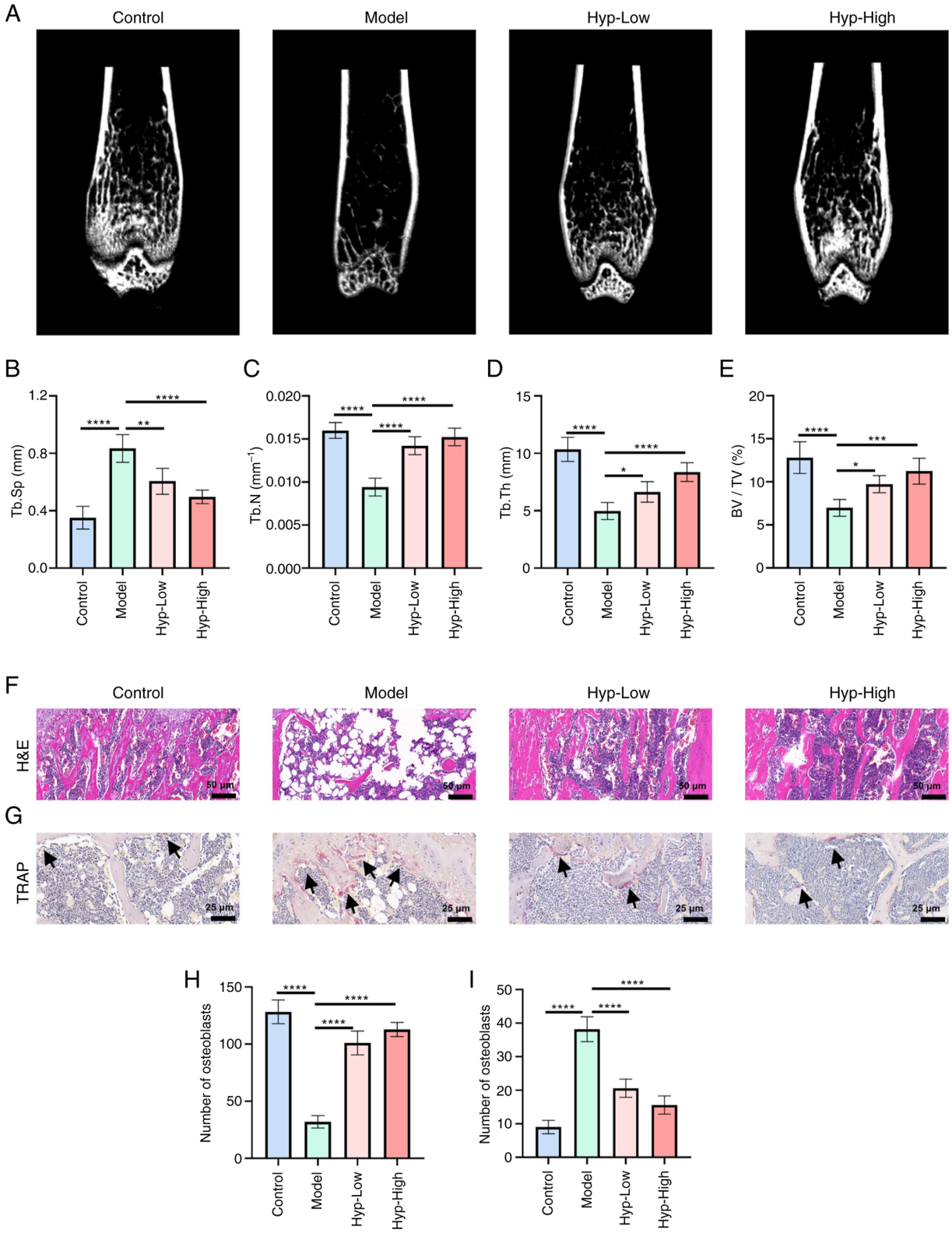

Figure 1. Hyp alleviates ovariectomy-induced osteoporosis in mice. (A) Representative micro-CT three-dimensional reconstruction images of the mouse femur. Quantitative analyses of (B) Tb.Sp, (C) Tb.N, (D) Tb.Th and (E) BV/TV (n=5). (F) Representative H&E staining images of femoral sections (n=5; x20 magnification). (G) Representative TRAP-stained sections showing osteoclasts (indicated by black arrows) (n=5; x40 magnification). (H) Quantification of osteoblast number per bone surface (n=5). (I) Quantification of osteoclast number per bone surface (n=5). Data are presented as the mean ± standard deviation. *P<0.05, **P<0.01, ***P<0.001 and ****P<0.0001. Tb.Sp, trabecular separation; Tb.N, trabecular number; Tb.Th, trabecular thickness; BV/TV, bone volume fraction; TRAP, tartrate-resistant acid phosphatase; Hyp, hyperoside.

The number of osteoblasts per bone surface was significantly decreased in the OVX model mice but was restored in a dose-dependent manner following Hyp treatment (Fig. 1H). Meanwhile, TRAP staining revealed a substantial increase

in TRAP-positive multinucleated osteoclasts in the OVX group, indicative of enhanced bone resorption (Fig. 1G and I). Notably, Hyp significantly reduced osteoclast numbers per bone surface compared with those in the OVX group. These results underscored the dual modulatory effects of Hyp on bone regulation, having simultaneously enhanced osteoblast activity and inhibited osteoclastogenesis, thereby contributing to the maintenance of bone homeostasis. Collectively, the present findings demonstrated that Hyp not only ameliorated microarchitectural deterioration associated with OP but also regulated key cellular mediators of bone remodeling, supporting its therapeutic potential in the management of OP.

Potential mechanism underlying the effects of Hyp on the treatment of OP. A volcano plot of the GSE35956 and GSE80614 gene expression datasets are shown in Fig. 2A. A total of 581 drug targets and 3,565 disease targets (Fig. 2B) were retrieved through online databases. By conducting an intersection analysis with a Venn diagram, 99 common target genes were determined and subsequently designated as potential therapeutic targets for further in-depth investigation (Fig. 2B). Subsequently, the STRING database was used to explore the potential associations among these 99 common genes. Subsequently, the analysis outcomes were imported into the Cytoscape software to generate a PPI network for Hyp in OP (Fig. 2C and D). In the degree value analysis of the PPI network, it was ascertained that the top 10 genes, namely *Src*, *Hsp90aa1*, *Akt1*, *Egfr*, *Tnf*, *Pik3ca*, *Bcl2*, *Grb2*, *Jak2* and *Erbb2*, were highly likely to assume a central role in the therapeutic process of Hyp for OP. Further GO molecular function analysis divulged that the top 5 functions of Hyp encompassed 'second-messenger-mediated signaling', maintenance of 'cellular calcium ion homeostasis', regulation of 'calcium ion homeostasis', 'response to molecule of bacterial origin' and 'regulation of cytosolic calcium ion concentration' (Fig. 2F). This implied that Hyp may have influenced intracellular signal transduction and ionic equilibrium by regulating these molecular functions, thereby exerting a beneficial effect on OP. Simultaneously, the KEGG enrichment analysis results demonstrated that pathways such as 'Prostate cancer', 'EGFR tyrosine kinase inhibitor resistance', 'PI3K-Akt signaling pathway', 'Neuroactive ligand-receptor interaction' and 'Human cytomegalovirus infection' held significant implications in the treatment of OP with Hyp (Fig. 2E).

Effect of Hyp on the viability of BMSCs. The chemical structure of Hyp is shown in Fig. 3A. The CCK-8 assay demonstrated that Hyp concentrations ≤40 μM did not exhibit significant cytotoxicity on BMSCs, with 20 and 40 μM selected for subsequent experiments (Fig. 3B). H_2O_2 at concentrations >100 μM significantly inhibited BMSC proliferation, and 200 μM H_2O_2 was chosen for inducing oxidative stress in BMSCs (Fig. 3C). Notably, Hyp effectively alleviated the inhibitory effect of H_2O_2 on BMSC proliferation (Fig. 3D). Further analysis using EDU labeling supported these findings. H_2O_2 treatment resulted in a reduced number of proliferating cells, as indicated by lower EDU incorporation (Fig. 3E). By contrast, Hyp treatment notably increased EDU-positive cells, suggesting its potential to promote BMSC proliferation under oxidative stress.

Hyp is capable of alleviating the oxidative stress induced by H_2O_2. The DCFH-DA staining outcomes manifested that upon the administration of H_2O_2, a conspicuous augmentation in fluorescence intensity was observed, signifying a pronounced elevation in the ROS levels within the cells (Fig. 4A and C). By contrast, when Hyp was introduced, a reduction in the fluorescence intensity of BMSCs ensued, implying a reduced ROS level. This was further corroborated by flow cytometry, wherein the average ROS levels were significantly elevated post-H_2O_2 treatment and subsequently decreased after Hyp treatment (Fig. 4B and D). Furthermore, the results of MDA detection assays indicated that H_2O_2 intervention led to a significant upsurge in MDA levels, whereas Hyp treatment effectively mitigated these levels (Fig. 4E). Similarly, the SOD detection assays revealed that H_2O_2 treatment induced a significant decline in SOD levels, which were significantly augmented following Hyp treatment (Fig. 4F). In summary, these comprehensive findings demonstrated that Hyp possessed the capacity to alleviate H_2O_2-induced oxidative stress levels in BMSCs. This not only holds promise for safeguarding cells against oxidative damage but also for maintaining cellular homeostasis, potentially providing new options for therapeutic interventions aimed at combating oxidative stress-related cellular dysfunctions.

Hyp protects the osteogenic differentiation ability of BMSCs. In the present study, the effect of Hyp on the osteogenic differentiation ability of BMSCs was investigated under oxidative stress conditions. The results of ALP and ARS staining assays demonstrated that the osteogenic differentiation capacity of BMSCs was significantly reduced after H_2O_2 intervention (Fig. 5A-D). However, treatment with Hyp significantly enhanced the osteogenic differentiation of BMSCs, as evidenced by the increased ALP activity and the greater number of calcium nodules detected by ARS staining. Furthermore, RT-qPCR analysis revealed that the expression levels of *Col1*, *Osterix*, *Runx2* and *Alp* were significantly decreased upon H_2O_2 exposure (Fig. 5E-H). By contrast, Hyp treatment led to a significant upregulation of these genes, indicating its positive regulatory role in osteogenic gene expression. Consistent with the RT-qPCR results, the results of western blot analysis also showed that Hyp treatment significantly increased the protein expression levels of Osterix and Runx2 (Fig. 5I-K). Collectively, these results provided compelling evidence that Hyp effectively protected the osteogenic differentiation ability of BMSCs under oxidative stress conditions, suggesting its potential therapeutic application in bone-related disorders associated with oxidative stress.

Hyp initiates activation of the PI3K/AKT signaling pathway. Western blot analysis of BMSCs revealed that H_2O_2 intervention led to a significant decline in the phosphorylation levels of both PI3K and AKT. By contrast, Hyp treatment effectively reversed this downward trend and promoted the activation of PI3K and AKT phosphorylation (Fig. 6A-C). This was further supported by immunohistochemical analysis of mouse femoral tissues, which indicated that the expression levels of p-PI3K and p-AKT were significantly

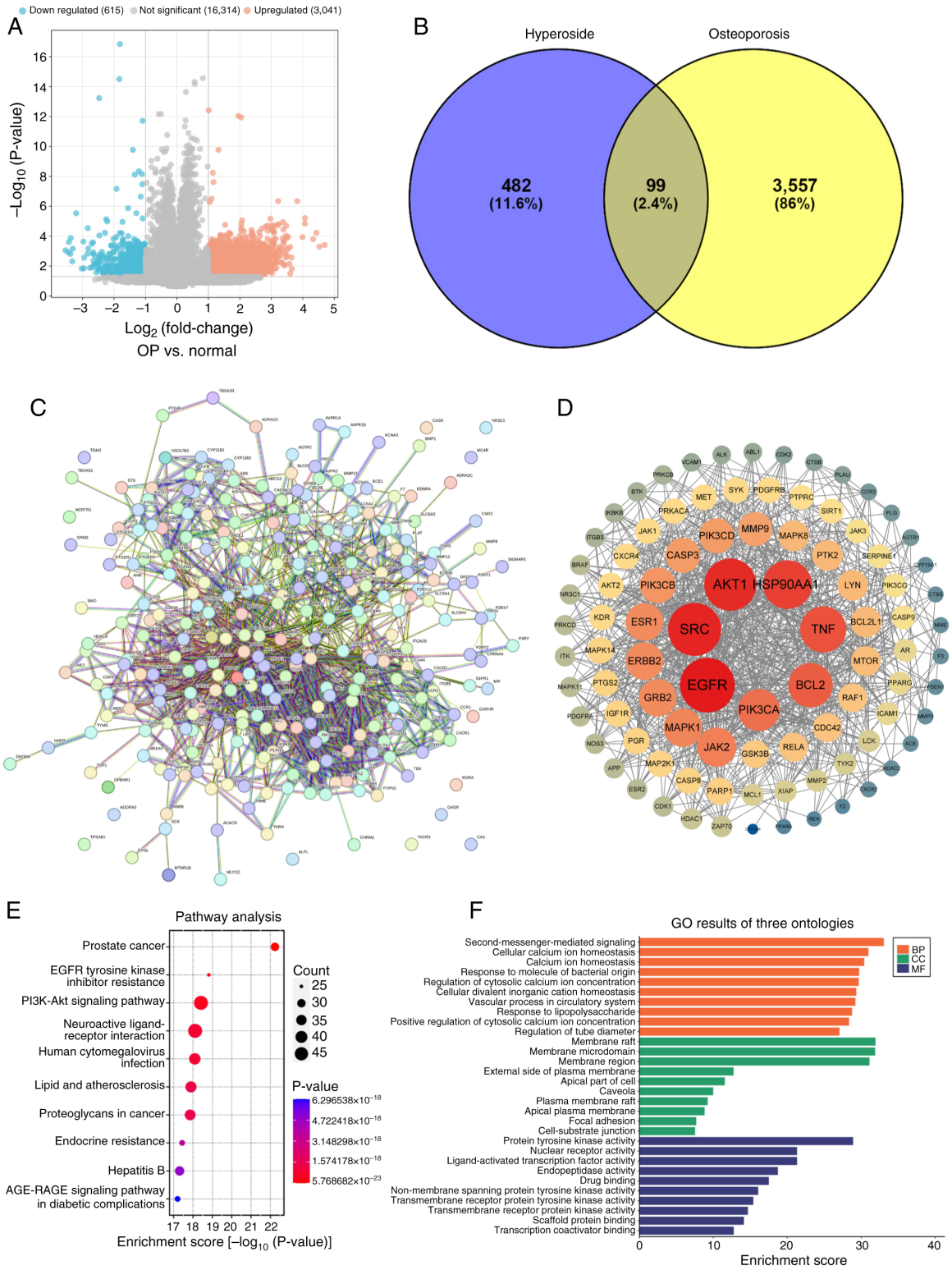

Figure 2. Potential mechanism of Hyperoside for the treatment of OP. (A) Volcano plots of the GSE35956 and GSE80614 gene chip datasets. (B) Venn diagram of disease and drug targets. (C) Protein-protein interaction network constructed using the STRING database of Hyperoside in the treatment of OP. (D) Visualization and analysis of the PPI network performed using Cytoscape software. (E) Bubble chart of Kyoto Encyclopedia of Genes and Genomes enrichment analysis. (F) GO enrichment analysis. All displayed GO terms met the significance threshold of adjusted P<0.05. OP, osteoporosis; GO, Gene Ontology; BP, biological process; CC, cellular component; MF, molecular function.

reduced in the model group compared with those in the control group (Fig. 6D-F). However, following Hyp intervention, a significant increase in the expression of p-PI3K and p-AKT was observed.

Inhibition of the PI3K/AKT pathway attenuates the antioxidative and osteogenic effects of Hyp. To investigate the role of the PI3K/AKT signaling pathway in the antioxidative and osteogenic effects of Hyp, a series of *in vitro* experiments

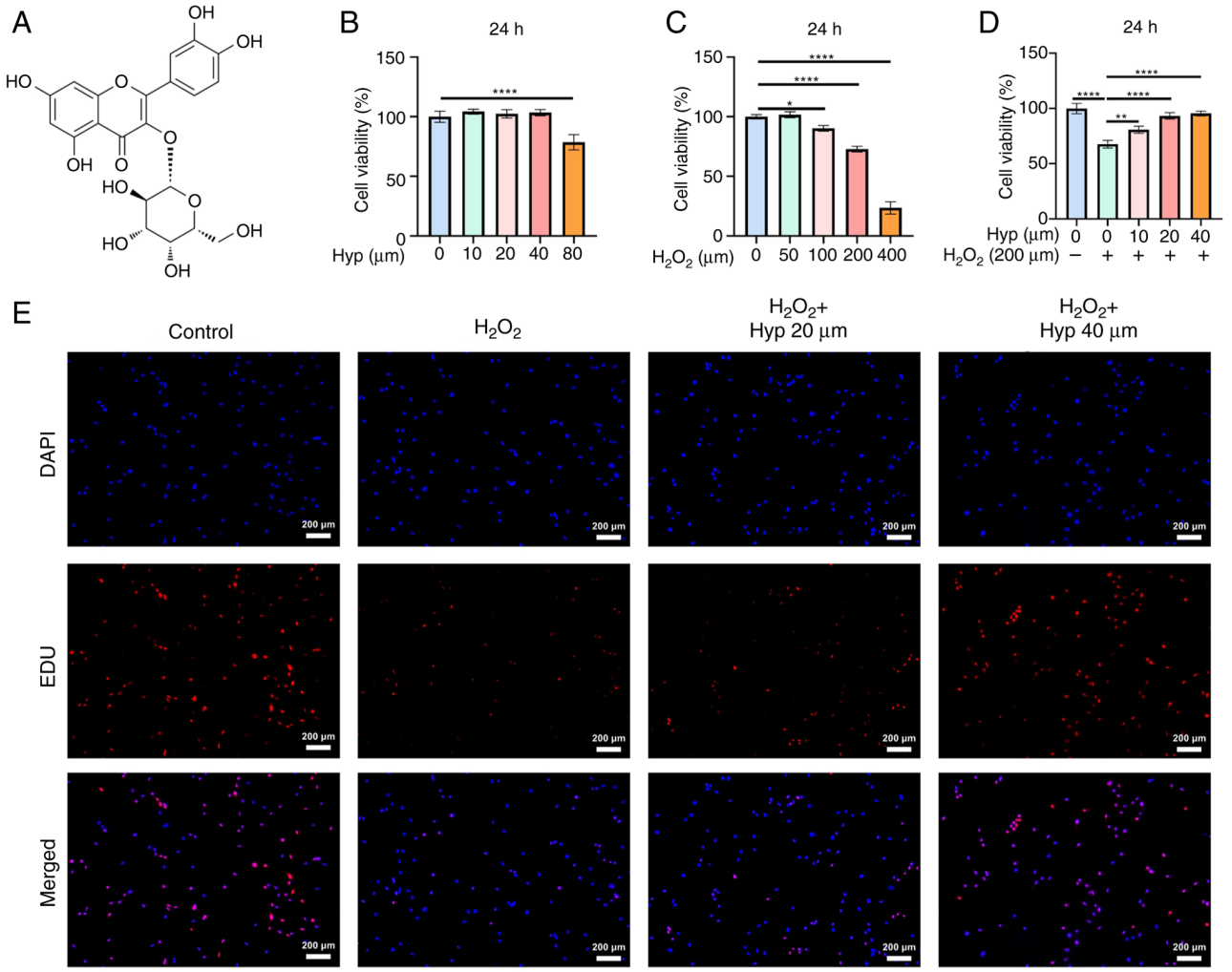

Figure 3. Hyp alleviates the inhibitory effect of H_2O_2 on the viability of BMSCs. (A) Chemical structure of Hyp. (B) Impact of Hyp on the viability of BMSCs (n=3). (C) Impact of H_2O_2 on the viability of BMSCs (n=3). (D) Impact of Hyp on the viability of BMSCs under the intervention of H_2O_2 (n=3). (E) Representative EDU staining images showing cell proliferation in BMSCs treated with Hyp and H_2O_2 (n=3; x5 magnification). Data are presented as the mean ± standard deviation. *P<0.05, **P<0.01 and ****P<0.0001. BMSC, bone marrow mesenchymal stem cells; Hyp, hyperoside.

were conducted using LY294002, a specific inhibitor of the PI3K/AKT pathway. LY294002 is a synthetic flavonoid derivative that acts as a reversible, ATP-competitive inhibitor of PI3Ks, thereby blocking the phosphorylation and subsequent activation of AKT and downstream signaling molecules. DCFH-DA fluorescence staining revealed that Hyp treatment significantly reduced H_2O_2-induced intracellular ROS levels, as evidenced by decreased green fluorescence intensity (Fig. 7A and B). However, co-treatment with LY294002 partially yet significantly restored the fluorescence signal and elevated ROS levels, suggesting that the antioxidative capacity of Hyp was impaired when the PI3K/AKT pathway was inhibited. Regarding osteogenic differentiation, ALP staining and enzyme activity assays demonstrated that Hyp significantly increased ALP activity, indicating the promotion of early osteogenesis (Fig. 7C and D). By contrast, the ALP activity and staining intensity were significantly reduced in the Hyp + LY294002 group, approaching the levels observed in the H_2O_2 group. These findings suggested that the PI3K/AKT pathway was involved in Hyp-induced early osteogenic differentiation. Furthermore, ARS staining showed a substantial increase in mineralized nodule formation in the Hyp-treated group, with quantitative analysis supporting elevated calcium deposition (Fig. 7E and F). However, in the Hyp + LY294002 group, both the ARS-stained area and calcium content were markedly decreased, indicating compromised osteogenic mineralization.

Western blot analysis corroborated these findings. Compared with in the model group, Hyp treatment significantly upregulated the expression levels of p-PI3K and p-AKT, as well as the key osteogenic transcription factors Runx2 and Osterix (Fig. 7G-K). By contrast, co-treatment with LY294002 resulted in a significant downregulation of these proteins, demonstrating that LY294002 partially reversed the effects of Hyp on PI3K/AKT signaling and its downstream targets. Collectively, these results indicated that Hyp exerted its antioxidative and pro-osteogenic effects by activating the PI3K/AKT signaling pathway and that inhibition of this pathway significantly attenuated its biological functions, highlighting the notable role of PI3K/AKT signaling in mediating the effects of Hyp.

Discussion

Oxidative stress has been acknowledged to serve an important role in the pathogenesis of OP, a view that has become

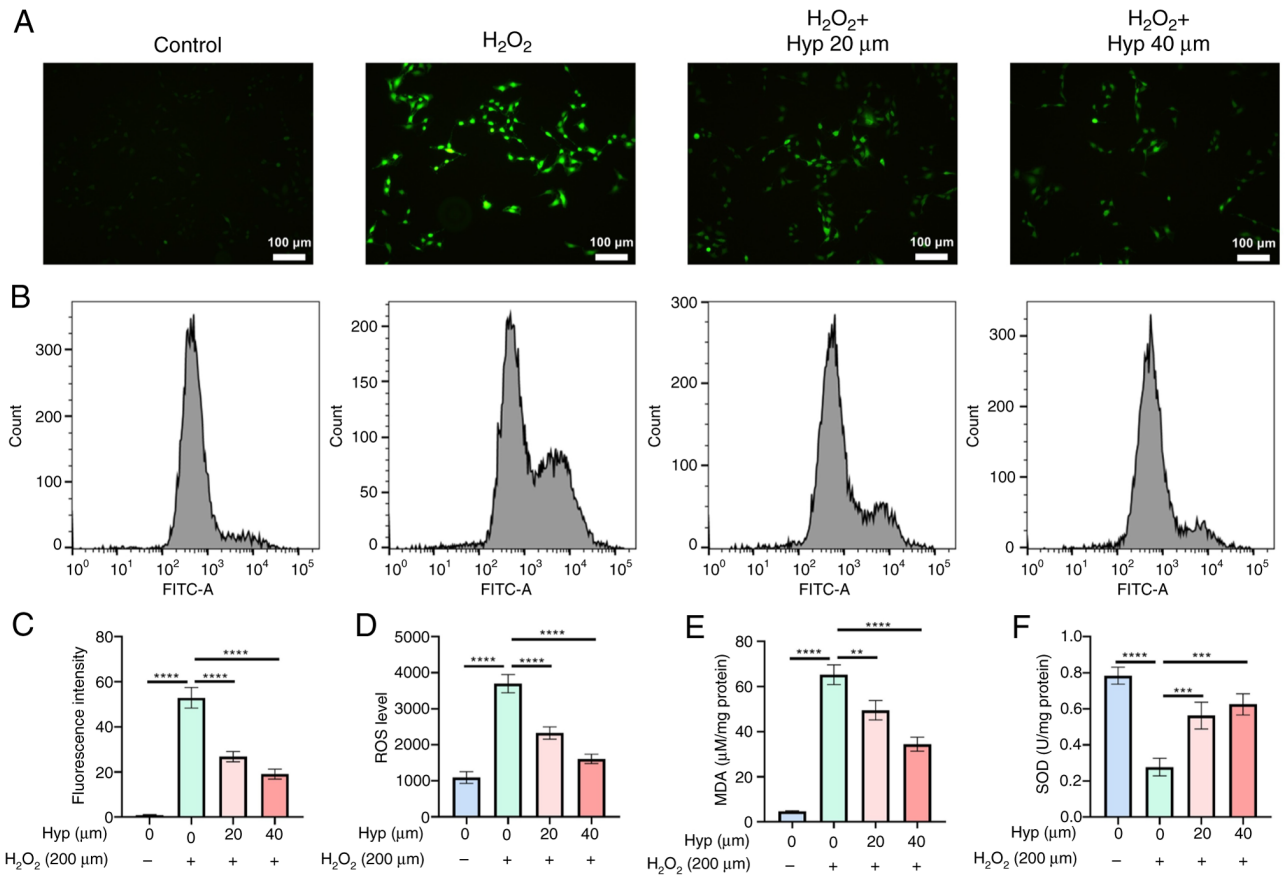

Figure 4. Hyperoside alleviates the oxidative stress of bone marrow mesenchymal stem cells induced by H_2O_2. (A) Representative fluorescence images of DCFH-DA staining (n=3; x10 magnification). (B) Representative flow cytometry images of DCFH-DA staining (n=3). (C) Quantification of the fluorescence intensity of DCFH-DA staining and (D) quantification of the mean fluorescence intensity in flow cytometry (n=3). Quantification of the (E) MDA and (F) SOD levels (n=3). Data are presented as the mean ± standard deviation. **P<0.01, ***P<0.001 and ****P<0.0001. Hyp, hyperoside; ROS, reactive oxygen species; MDA, malondialdehyde; SOD, superoxide dismutase.

accepted in the current research field (11). With increases in age, alterations in hormonal levels and the influence of other pathological factors, the redox balance within the body is disrupted, leading to the excessive generation of oxidative stress products such as ROS (10,25) ROS can target intracellular biomacromolecules, resulting in lipid peroxidation, protein oxidative modification and DNA damage, thereby impairing the normal function and viability of cells (26). In the skeletal system, oxidative stress can markedly enhance the activity and number of osteoclasts, thereby promoting the bone resorption process. Concurrently, it inhibits the proliferation, differentiation and mineralization capacity of osteoblasts, ultimately reducing bone formation. This disruption in the balance of bone remodeling leads to bone mass loss, and the occurrence and development of OP (27). A large number of *in vivo* and *in vitro* studies have provided conclusive evidence for this, prompting researchers to continuously explore effective antioxidant strategies to combat OP (28,29).

Hyp is a natural flavanol glycoside compound that has been shown to possess notable antioxidant and anti-inflammatory activities (30,31). A study conducted by Chen *et al* (19) demonstrated that Hyp can prevent oxidative stress-induced liver injury in rats. Additionally, Wu *et al* (32) revealed that Hyp can treat acute kidney injury by regulating oxidative stress and cell apoptosis. These findings collectively support the potent antioxidant therapeutic effects of Hyp.

The present study found that Hyp exhibits a notable ability to alleviate oxidative stress. The results of DCFH-DA staining to measure the intracellular ROS levels showed that the fluorescence intensity of the cells was significantly reduced after Hyp treatment, indicating that Hyp effectively decreased intracellular ROS generation. Meanwhile, the detection of MDA content showed that Hyp reduced the MDA levels, and the detection of SOD activity indicated that Hyp enhanced SOD activity. This further supported the role of Hyp in alleviating oxidative stress from the perspectives of lipid peroxidation levels and the antioxidant enzyme system. This ability to reduce oxidative stress is of notable importance for protecting cells from oxidative damage, especially for cell types such as BMSCs that have a key role in bone metabolism, thereby providing a favorable microenvironment for maintaining their normal osteogenic differentiation ability.

Oxidative stress refers to a state in which the body, when exposed to various harmful stimuli, produces an excessive amount of highly reactive molecules such as ROS and reactive nitrogen species, leading to an imbalance between the oxidative system and the antioxidant system, and ultimately causing damage to cells and tissues (33,34). Excessive oxidative stress can cause a notable accumulation of ROS within cells,

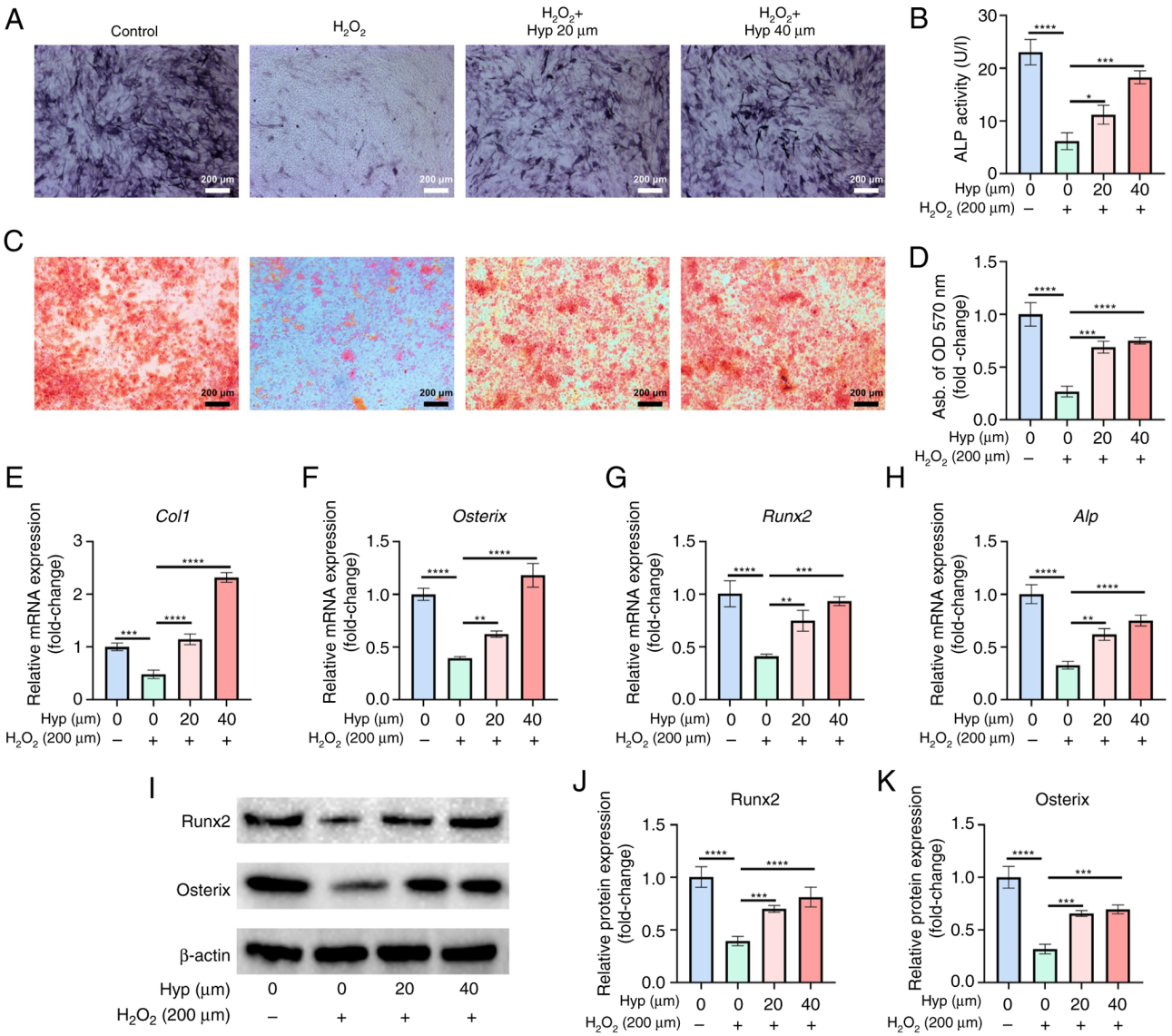

Figure 5. Hyperoside rescues the osteogenic differentiation function of bone marrow mesenchymal stem cells. (A) Representative images of ALP staining and (B) quantification of ALP activity (n=3; x5 magnification). (C) Representative images of ARS staining and (D) quantification of ARS staining (n=3; x5 magnification). The mRNA expression levels of (E) *Col1*, (F) *Osterix*, (G) *Runx2* and (H) *Alp* (n=3). (I) Representative western blot images, and semi-quantification of the protein expression levels of (J) Runx2 and (K) Osterix (n=3). Data are presented as the mean ± standard deviation. *P<0.05, **P<0.01, ***P<0.001 and ****P<0.0001. OD, optical density; Hyp, Hyperoside; *Col1*, type-I collagen; Runx2, runt-related transcription factor 2; ARS, Alizarin red S; ALP/*Alp*, alkaline phosphatase.

inflicting damage on cellular DNA. DNA damage may trigger cell cycle arrest, thereby preventing osteoblast precursor cells from undergoing normal mitosis and differentiation. Severe DNA damage can also lead to cell apoptosis, reducing the number of osteoblasts and thus inhibiting osteogenic differentiation (35).Therefore, enhancing the antioxidant capacity and osteogenic differentiation ability of BMSCs is an important research direction for the treatment of OP.

The results of the present study indicated that Hyp not only reduced oxidative stress but also had a significant protective effect on the osteogenic differentiation ability of BMSCs. In the ALP and ARS staining experiments, the ALP activity of the Hyp-treated group was significantly enhanced, and the ARS staining showed a significant increase in the number of calcium nodules, which are important markers of enhanced osteogenic differentiation. At the molecular level, RT-qPCR and western blot analysis revealed that Hyp upregulated the expression of osteogenic-related genes and proteins, such as *Col1, Osterix, Runx2* and *Alp*. This series of results clearly demonstrated the positive role of Hyp in protecting and promoting the osteogenic differentiation of BMSCs. The mechanism of action of Hyp may have involved reducing the interference of oxidative stress on intracellular signal pathways, thus maintaining the normal transduction of osteogenic differentiation-related signals, enabling BMSCs to differentiate into osteoblasts in a relatively stable environment and providing a strong cellular basis for bone formation.

The PI3K/AKT signaling pathway, an important intracellular signal transduction pathway, serves a central role in the regulation of oxidative stress and OP, a concept that is widely accepted in current research (29,36). The activation of the PI3K/AKT signaling pathway can alleviate oxidative

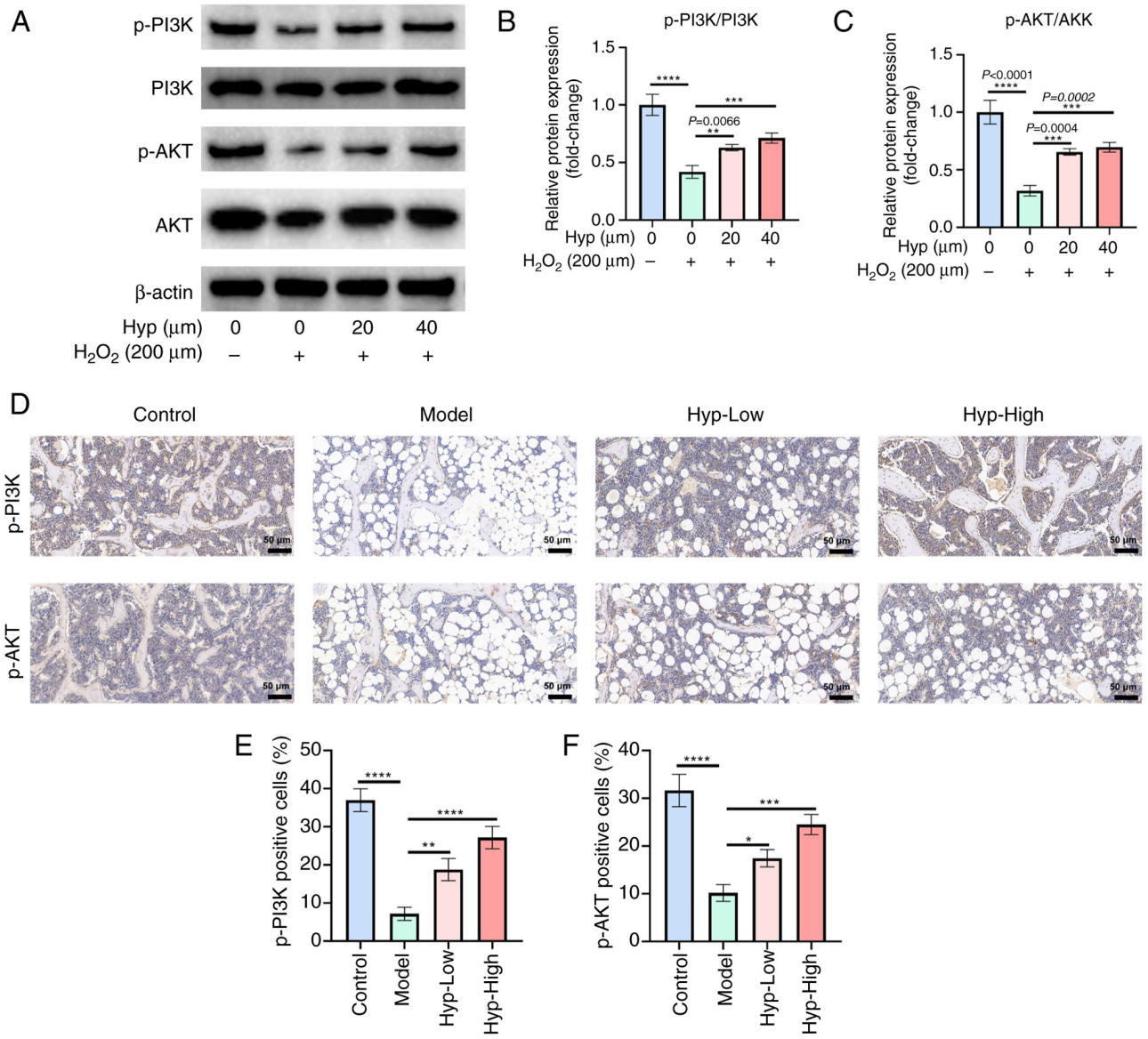

Figure 6. Hyp initiates activation of the PI3K/AKT signaling pathway. (A) Representative western blotting images, and semi-quantification of the protein expression levels of (B) p-PI3K/PI3K and (C) p-AKT/AKT (n=3). (D) Representative immunohistochemistry images of p-PI3K and p-AKT expression in femoral sections. Semi-quantification of (E) p-PI3K- and (F) p-AKT-positive cells observed in (D) (n=5; x20 magnification). Data are presented as the mean ± standard deviation. *P<0.05, **P<0.01, ***P<0.001 and ****P<0.0001. Hyp, Hyperoside; p-, phosphorylated.

stress through various mechanisms, including upregulating the expression of antioxidant enzyme genes, enhancing the synthesis of intracellular antioxidant substances and inhibiting the activity of enzymes related to ROS production, thus maintaining the intracellular redox balance (37,38). In terms of bone metabolism, the activation of the PI3K/AKT signaling pathway can promote the proliferation, differentiation and survival of osteoblasts, while inhibiting osteoclast activity, thus preserving the normal process of bone remodeling and regulating OP (39,40). For instance, Wu *et al* (41) demonstrated that 7,8-dihydroxyflavone can inhibit oxidative stress and promote bone formation by activating the tyrosine kinase receptor B/PI3K/AKT pathway. This pathway enhances the viability and osteogenic differentiation ability of BMSCs inhibited by H_2O_2-induced oxidative stress, thereby improving OP (28). Several other natural compounds, such as luteolin and curcumin, have also been reported to regulate bone metabolism through the PI3K/AKT pathway (42,43). While luteolin similarly promotes osteoblast differentiation via the PI3K/AKT signaling pathway, evidence regarding its role in redox regulation remains limited (29). Curcumin has been shown to promote osteogenic differentiation in association with PI3K/AKT and nuclear factor erythroid 2-related factor 2 (Nrf2) activation, suggesting a role in both bone formation and antioxidative responses (43).

By contrast, the present study showed that Hyp exerted both antioxidative and osteogenic effects in a PI3K/AKT-dependent manner, highlighting its dual-function specificity and potential novelty. In the present study, Hyp significantly activated the PI3K/AKT signaling pathway. Western blot analysis revealed that Hyp treatment partially reversed the H_2O_2-induced reduction in p-PI3K and p-AKT levels, and immunohistochemical staining further supported

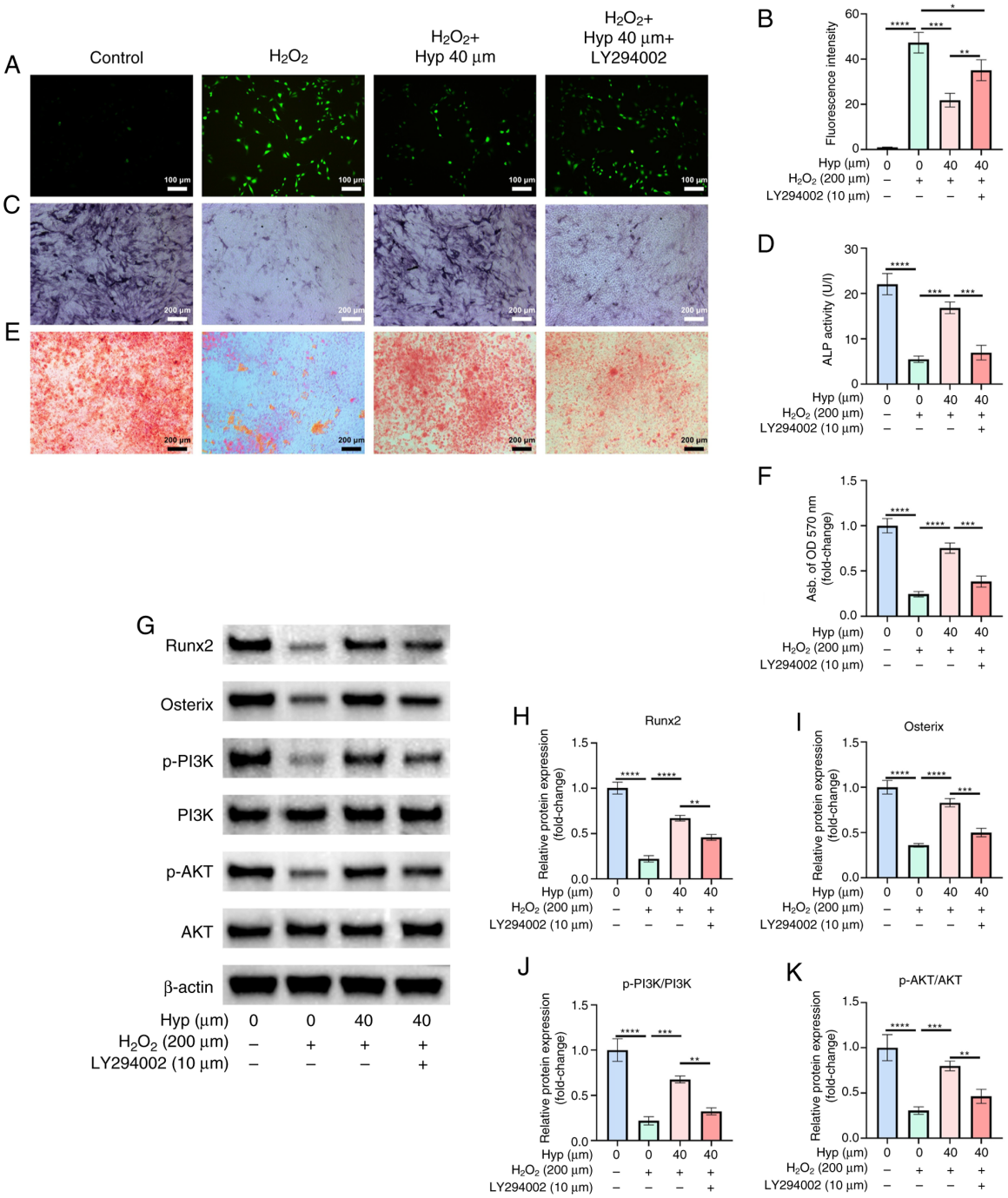

Figure 7. Inhibition of the PI3K/AKT pathway attenuates the antioxidative and osteogenic effects of Hyp. (A) Representative fluorescence images of DCFH-DA staining and (B) quantification (n=3; x10 magnification). (C) Representative images of ALP staining and (D) quantification of ALP activity (n=3; x5 magnification). (E) Representative images of ARS staining and (F) quantification of ARS absorbance levels (n=3; x5 magnification). (G) Representative western blotting images, and semi-quantification of the protein expression levels of (H) Runx2, (I) Osterix, (J) p-PI3K/PI3K and (K) p-AKT/AKT (n=3). Data are presented as the mean ± standard deviation. *P<0.05, **P<0.01, ***P<0.001 and ****P<0.0001. Hyp, Hyperoside; ALP, alkaline phosphatase; ARS, Alizarin red S; Runx2, runt-related transcription factor 2; p-, phosphorylated.

the upregulation of p-PI3K and p-AKT expression following Hyp administration. These results suggested that Hyp exerted both antioxidative and osteogenic effects at least in part through PI3K/AKT pathway activation.

To validate the specificity of this signaling axis, the present study employed LY294002, a classical PI3K inhibitor, and showed that co-treatment with LY294002 significantly attenuated the beneficial effects of Hyp. Specifically, the reduction of ROS levels by Hyp, as evidenced by DCFH-DA staining, was partially reversed by LY294002, indicating a decline in the antioxidative efficacy of Hyp. Similarly, ALP staining, ALP activity and ARS staining demonstrated that LY294002 co-treatment inhibited Hyp-induced early- and late-stage osteogenesis. Western blot analysis further supported that LY294002 significantly suppressed the Hyp-induced upregulation of p-PI3K, p-AKT and key osteogenic transcription factors, such as Runx2 and Osterix. These findings collectively suggested that the PI3K/AKT pathway was not only activated

by Hyp but was also important for its antioxidative and osteogenic actions. The use of LY294002 as a pathway-specific inhibitor provided robust mechanistic evidence supporting the notable role of PI3K/AKT in mediating the therapeutic effects of Hyp. These results align with prior studies highlighting the importance of this pathway in OP treatment and offer a more comprehensive mechanistic understanding of the pharmacological profile of Hyp (44,45).

In summary, the results of the present study indicated that Hyp holds notable promise in the treatment of OP and suggested that its mechanism of action was multifaceted. The results indicated that Hyp promoted bone homeostasis through multiple mechanisms, including mitigating oxidative stress, preserving osteogenic differentiation capacity and activating the PI3K/AKT signaling pathway. These findings provide a solid theoretical basis for further development of Hyp-based therapeutic strategies for OP.

However, the present study also had certain limitations. Firstly, the present study was mainly based on cell and animal experimental models. Although these models can provide important information regarding the mechanism of Hyp action, the physiological environment and disease state of the human body are notably complex. The efficacy, safety and pharmacokinetic characteristics of Hyp in humans remain to be verified through further clinical studies. Secondly, although the present study has preliminarily revealed the association between Hyp and the PI3K/AKT signaling pathway, the upstream and downstream molecular regulatory networks of this pathway, as well as its potential crosstalk with other signaling pathways, remain insufficiently elucidated. Notably, it remains to be fully elucidated whether Hyp directly regulates other redox-sensitive pathways such as the ROS/Kelch-like ECH-associated protein 1/Nrf2 axis, which serves a central role in maintaining intracellular oxidative balance in bone-related cells. Therefore, further in-depth studies using targeted molecular approaches, such as pathway-specific inhibitors, activators or genetic knockdown models, are necessary to comprehensively uncover the mechanistic landscape of the biological activity of Hyp. Thirdly, the present study did not evaluate serum calcium and estrogen levels. Direct biochemical measurements would provide stronger support for the pathophysiological relevance and treatment efficacy of Hyp. Future investigations should incorporate these assessments to strengthen the comprehensiveness and translational relevance of findings.

Acknowledgements

Not applicable.

Funding

The present study was supported by the Science and Technology Projects for Social Development in Dongguan City (grant no. 20221800900102).

Availability of data and materials

The datasets used or analyzed during the current study are available from the corresponding author on reasonable request.

Authors' contributions

LL and DX designed the study. LL and DX wrote the manuscript. LL, HD and SZ performed animal experiments. LL and HD carried out online data information collection. LL, HD, SZ and BW performed the cell experiments. LL and DX performed the statistical analysis. DX revised the manuscript. LL and DX confirm the authenticity of all the raw data. All authors read and approved the final version of the manuscript.

Ethics approval and consent to participate

All animal experimental procedures were approved by the Animal Experiment Ethics Committee of The First Affiliated Hospital of Guangzhou University of Chinese Medicine (approval no. GZTCMF1-202403241) and were performed in accordance with institutional and national guidelines for the care and use of laboratory animals. According to the ethics committee, the commercially purchased mouse primary BMSCs used in the present study did not require additional ethics approval.

Patient consent for publication

Not applicable.

Competing interests

The authors declare that they have no competing interests.

References

1. Walker MD and Shane E: Postmenopausal osteoporosis. N Engl J Med 389: 1979-1991, 2023.
2. Tang SS, Yin XJ, Yu W, Cui L, Li ZX, Cui LJ, Wang LH and Xia W: Prevalence of osteoporosis and related factors in postmenopausal women aged 40 and above in China. Zhonghua Liu Xing Bing Xue Za Zhi 43: 509-516, 2022 (In Chinese).
3. LeBoff MS, Greenspan SL, Insogna KL, Lewiecki EM, Saag KG, Singer AJ and Siris ES: The clinician's guide to prevention and treatment of osteoporosis. Osteoporos Int 33: 2049-2102, 2022.
4. Cosman F, Langdahl B and Leder BZ: Treatment sequence for osteoporosis. Endocr Pract 30: 490-496, 2024.
5. Eid A and Atlas J: The role of bisphosphonates in medical oncology and their association with jaw bone necrosis. Oral Maxillofac Surg Clin North Am 26: 231-237, 2014.
6. Chlebowski RT and Manson JE: Menopausal hormone therapy and breast cancer. Cancer J 28: 169-175, 2022.
7. Cho L, Kaunitz AM, Faubion SS, Hayes SN, Lau ES, Pristera N, Scott N, Shifren JL, Shufelt CL, Stuenkel CA, *et al*: Rethinking menopausal hormone therapy: For whom, what, when, and how long? Circulation 147: 597-610, 2023.
8. Luo J, Mills K, le Cessie S, Noordam R and van Heemst D: Ageing, age-related diseases and oxidative stress: What to do next? Ageing Res Rev 57: 100982, 2020.
9. Iantomasi T, Romagnoli C, Palmini G, Donati S, Falsetti I, Miglietta F, Aurilia C, Marini F, Giusti F and Brandi ML: Oxidative stress and inflammation in osteoporosis: Molecular mechanisms involved and the relationship with microRNAs. Int J Mol Sci 24: 3772, 2023.
10. Marcucci G, Domazetovic V, Nediani C, Ruzzolini J, Favre C and Brandi ML: Oxidative stress and natural antioxidants in osteoporosis: Novel preventive and therapeutic approaches. Antioxidants (Basel) 12: 373, 2023.
11. Kimball JS, Johnson JP and Carlson DA: Oxidative stress and osteoporosis. J Bone Joint Surg Am 103: 1451-1461, 2021.
12. Chen Y, Cai Y, Chen C, Li M, Lu L, Yu Z, Wang S, Fang L and Xu S: Aroclor 1254 induced inhibitory effects on osteoblast differentiation in murine MC3T3-E1 cells through oxidative stress. Front Endocrinol (Lausanne) 13: 940624, 2022.

13. Tanaka M, Inoue H, Takahashi N and Uehara M: AMPK negatively regulates RANKL-induced osteoclast differentiation by controlling oxidative stress. Free Radic Biol Med 205: 107-115, 2023.
14. Zhu C, Shen S, Zhang S, Huang M, Zhang L and Chen X: Autophagy in bone remodeling: A regulator of oxidative stress. Front Endocrinol (Lausanne) 13: 898634, 2022.
15. Zhao Q, Feng J, Liu F, Liang Q, Xie M, Dong J, Zou Y, Ye J, Liu G, Cao Y, *et al*: Rhizoma Drynariae-derived nanovesicles reverse osteoporosis by potentiating osteogenic differentiation of human bone marrow mesenchymal stem cells via targeting ERα signaling. Acta Pharm Sin B 14: 2210-2227, 2024.
16. Li B, Wang Y, Gong S, Yao W, Gao H, Liu M and Wei M: Puerarin improves OVX-induced osteoporosis by regulating phospholipid metabolism and biosynthesis of unsaturated fatty acids based on serum metabolomics. Phytomedicine 102: 154198, 2022.
17. Rao T, Tong H, Li J, Huang J, Yin Y and Zhang J: Exploring the role and mechanism of hyperoside against cardiomyocyte injury in mice with myocardial infarction based on JAK2/STAT3 signaling pathway. Phytomedicine 128: 155319, 2024.
18. Zhao K, Zhou F, Lu Y, Gao T, Wang R, Xie M and Wang H: Hyperoside alleviates depressive-like behavior in social defeat mice by mediating microglial polarization and neuroinflammation via TRX1/NLRP1/Caspase-1 signal pathway. Int Immunopharmacol 145: 113731, 2025.
19. Chen Y, Dai F, He Y, Chen Q, Xia Q, Cheng G, Lu Y and Zhang Q: Beneficial effects of hyperoside on bone metabolism in ovariectomized mice. Biomed Pharmacother 107: 1175-1182, 2018.
20. Yan K, Zhang RK, Wang JX, Chen HF, Zhang Y, Cheng F, Jiang Y, Wang M, Wu Z, Chen XG, *et al*: Using network pharmacology and molecular docking technology, proteomics and experiments were used to verify the effect of Yigu decoction (YGD) on the expression of key genes in osteoporotic mice. Ann Med 57: 2449225, 2025.
21. Yang PH, Wei YN, Xiao BJ, Li SY, Li XL, Yang LJ, Pan HF and Chen GX: Curcumin for gastric cancer: Mechanism prediction via network pharmacology, docking, and in vitro experiments. World J Gastrointest Oncol 16: 3635-3650, 2024.
22. Benisch P, Schilling T, Klein-Hitpass L, Frey SP, Seefried L, Raaijmakers N, Krug M, Regensburger M, Zeck S, Schinke T, *et al*: The transcriptional profile of mesenchymal stem cell populations in primary osteoporosis is distinct and shows overexpression of osteogenic inhibitors. PLoS One 7: e45142, 2012.
23. van de Peppel J, Strini T, Tilburg J, Westerhoff H, van Wijnen AJ and van Leeuwen JP: Identification of three early phases of cell-fate determination during osteogenic and adipogenic differentiation by transcription factor dynamics. Stem Cell Reports 8: 947-960, 2017.
24. Livak KJ and Schmittgen TD: Analysis of relative gene expression data using real-time quantitative PCR and the 2(-Delta Delta C(T)) method. Methods 25: 402-408, 2001.
25. Zhang C, Li H, Li J, Hu J, Yang K and Tao L: Oxidative stress: A common pathological state in a high-risk population for osteoporosis. Biomed Pharmacother 163: 114834, 2023.
26. Karthik V and Guntur AR: Energy metabolism of osteocytes. Curr Osteoporos Rep 19: 444-451, 2021.
27. Shinohara I, Morita M, Chow SK, Murayama M, Sususki Y, Gao Q and Goodman SB: Pathophysiology of the effects of oxidative stress on the skeletal system. J Orthop Res 43: 1059-1072, 2025.
28. Li D, Zhao Z, Zhu L, Feng H, Song J, Fu J, Li J, Chen Z and Fu H: 7,8-DHF inhibits BMSC oxidative stress via the TRKB/PI3K/AKT/NRF2 pathway to improve symptoms of postmenopausal osteoporosis. Free Radic Biol Med 223: 413-429, 2024.
29. Chai S, Yang Y, Wei L, Cao Y, Ma J, Zheng X, Teng J and Qin N: Luteolin rescues postmenopausal osteoporosis elicited by OVX through alleviating osteoblast pyroptosis via activating PI3K-AKT signaling. Phytomedicine 128: 155516, 2024.
30. Jang E: Hyperoside as a potential natural product targeting oxidative stress in liver diseases. Antioxidants (Basel) 11: 1437, 2022.
31. Ku SK, Zhou W, Lee W, Han MS, Na M and Bae JS: Anti-inflammatory effects of hyperoside in human endothelial cells and in mice. Inflammation 38: 784-799, 2015.
32. Wu L, Li Q, Liu S, An X, Huang Z, Zhang B, Yuan Y and Xing C: Protective effect of hyperoside against renal ischemia-reperfusion injury via modulating mitochondrial fission, oxidative stress, and apoptosis. Free Radic Res 53: 727-736, 2019.
33. Lennicke C and Cocheme HM: Redox metabolism: ROS as specific molecular regulators of cell signaling and function. Mol Cell 81: 3691-3707, 2021.
34. Gebicki JM: Oxidative stress, free radicals and protein peroxides. Arch Biochem Biophys 595: 33-39, 2016.
35. Jomova K, Raptova R, Alomar SY, Alwasel SH, Nepovimova E, Kuca K and Valko M: Reactive oxygen species, toxicity, oxidative stress, and antioxidants: chronic diseases and aging. Arch Toxicol 97: 2499-2574, 2023.
36. Ren BC, Zhang YF, Liu SS, Cheng XJ, Yang X, Cui XG, Zhao XR, Zhao H, Hao MF, Li MD, *et al*: Curcumin alleviates oxidative stress and inhibits apoptosis in diabetic cardiomyopathy via Sirt1-Foxo1 and PI3K-Akt signalling pathways. J Cell Mol Med 24: 12355-12367, 2020.
37. Deng S, Dai G, Chen S, Nie Z, Zhou J, Fang H and Peng H: Dexamethasone induces osteoblast apoptosis through ROS-PI3K/AKT/GSK3β signaling pathway. Biomed Pharmacother 110: 602-608, 2019.
38. Wei L, Chen W, Huang L, Wang H, Su Y, Liang J, Lian H, Xu J, Zhao J and Liu Q: Alpinetin ameliorates bone loss in LPS-induced inflammation osteolysis via ROS mediated P38/PI3K signaling pathway. Pharmacol Res 184: 106400, 2022.
39. Xin L, Feng HC, Zhang Q, Cen XL, Huang RR, Tan GY and Zhang Q: Exploring the osteogenic effects of simiao wan through activation of the PI3K/AKT pathway in osteoblasts. J Ethnopharmacol 338: 119023, 2025.
40. Wang D, Liu Y, Tang D, Wei S, Sun J, Ruan L, He L, Li R, Ren Q, Tian X and Chen Y: Induction of PI3K/Akt-mediated apoptosis in osteoclasts is a key approach for buxue tongluo pills to treat osteonecrosis of the femoral head. Front Pharmacol 12: 729909, 2021.
41. Wu CH, Hung TH, Chen CC, Ke CH, Lee CY, Wang PY and Chen SF: Post-injury treatment with 7,8-dihydroxyflavone, a TrkB receptor agonist, protects against experimental traumatic brain injury via PI3K/Akt signaling. PLoS One 9: e113397, 2014.
42. Liang G, Zhao J, Dou Y, Yang Y, Zhao D, Zhou Z, Zhang R, Yang W and Zeng L: Mechanism and experimental verification of luteolin for the treatment of osteoporosis based on network pharmacology. Front Endocrinol (Lausanne) 13: 866641, 2022.
43. Xiong Y, Zhao B, Zhang W, Jia L, Zhang Y and Xu X: Curcumin promotes osteogenic differentiation of periodontal ligament stem cells through the PI3K/AKT/Nrf2 signaling pathway. Iran J Basic Med Sci 23: 954-960, 2020.
44. Lu J, Shi X, Fu Q, Han Y, Zhu L, Zhou Z, Li Y and Lu N: New mechanistic understanding of osteoclast differentiation and bone resorption mediated by P2X7 receptors and PI3K-Akt-GSK3beta signaling. Cell Mol Biol Lett 29: 100, 2024.
45. Jiang Z, Deng L, Li M, Alonge E, Wang Y and Wang Y: Ginsenoside Rg1 modulates PI3K/AKT pathway for enhanced osteogenesis via GPER. Phytomedicine 124: 155284, 2024.